Highly Ordered Nanometer-Scale Chemical and Protein Patterns by Binary Colloidal Crystal Lithography Combined with Plasma Polymerization

ARTICLE *in* ADVANCED FUNCTIONAL MATERIALS · FEBRUARY 2011

Impact Factor: 11.81 · DOI: 10.1002/adfm.201001340

ADVANCED FUNCTIONAL MATERIALS
www.afm-journal.de

Highly Ordered Nanometer-Scale Chemical and Protein Patterns by Binary Colloidal Crystal Lithography Combined with Plasma Polymerization

*Gurvinder Singh, Hans J. Griesser, Kristen Bremmell, and Peter Kingshott**

Surfaces with micro- and nanometer-scale patterns have many potential applications, particularly in lifescience. This article reports on a versatile, straightforward, and inexpensive approach for the creation of chemical patterns using fabricated binary colloid crystals, consisting of small and large particles, as masks for the deposition of an amino-functionalised ultrathin film by plasma polymerization. After removal of the binary colloidal mask, the characterization techniques [scanning electron microscopy (SEM) and atomic force microscopy (AFM)] reveal a surface contrast that depicts an ability of the small particles to allow diffusion of the plasma to the substrate. A plasma-polymer film is created under the small particles and the region of substrate in direct contact with the large particle remains uncoated. Numerous types of patterns and feature heights can be produced with good fidelity over areas of several cm^2 by appropriate tuning of the binary colloid crystal mask morphology and the plasma-polymer deposition time. Finally, the amine groups of the patterned surface are used for covalent grafting poly(ethylene glycol) propionaldehyde (PEG-PALD) by reductive amination under conditions of reduced solubility to produce a patterned surface for directed adsorption of protein. AFM investigations show that the proteins are preferentially attached to the nanometer-scale regions of the pattern without PEG-PALD.

1. Introduction

The generation of surfaces with nanometer-scale chemical contrast and controlled morphology is of considerable interest for a wide range of applications in electronic,[1] magnetic,[2] chemical,[3] and biological sensors.[4] In particular, nano-engineered surfaces enable the study of fundamental aspects of cell adhesion at the level of single biomolecules such as proteins,[5] tissue engineering,[6] and artificial growth of neuronal networks.[7] The immobilization of single biomolecules with high spatial precision still imposes challenges. It requires the fabrication of chemical patterns with dimensions well below 100 nm, but would offer an avenue towards enhanced detection sensitivity with reduced quantities of analytes and reagents, and increased density of sensing elements on biochips.[8]

Chemical patterns can be created from organic molecules, polymers, biomolecules, or metal deposition onto a substrate. Several techniques have been investigated, producing chemically patterned surfaces for various applications. Among them, parallel processes such as photolithography, scanning near-field lithography, and soft lithography are capable of fabricating surfaces over a large area with high throughput, but are inadequate for achieving sub-100-nm or single-molecule resolution.[9–11] In contrast, dip-pen lithography and electron-beam lithography have been successfully applied to produce nanopatterns with sub-100-nm resolution, but they yield low throughput because of the slow serial processes involved.[12,13] These methods also impose some constraints, because they require complex instrumentation not available to many researchers. An approach yielding sub-100-nm nanopatterns with self-assembled monolayers (SAMs) without utilizing lithography techniques has recently been reported.[14] This method of nanopatterning is, however, restricted to a limited number of substrates, such as silicon for silane SAMs and gold for thiol or disulfide SAMs.

Recently, colloidal lithography has been developed as a versatile approach for the generation of nanometer-scale chemical patterns spanning large areas. This method exploits the self-assembly of two-dimensional (2D) monolayers of spherical particles as a mask and has been used to decorate substrate surfaces with metal,[15] catalysts,[16] polymers,[17] and inorganic materials.[18] Colloidal lithography can also be applied to attain nanometer-scale biomolecular patterning following chemical modification of the patterned surfaces, or directly to

G. Singh, Prof. P. Kingshott[+]
Interdisciplinary Nanoscience Center (iNANO)
University of Aarhus
Ny Munkegade, Building 1521, 8000 Aarhus C, Denmark
E-mail: peter.kingshott@inano.dk
Prof. H. J. Griesser
Ian Wark Research Institute
University of South Australia
Mawson Lakes, Adelaide 5091, Australia
Dr. K. Bremmell
School of Pharmacy and Medical Science
University of South Australia
Adelaide 5000, Australia
[+] Present Address: Faculty of Engineering and Industrial Sciences, Swinburne University of Technology, Hawthorn, 3122 VIC, Australia

DOI: 10.1002/adfm.201001340

form periodic arrays of protein nanostructures.[19,20] Colloidal lithography combined with a plasma polymerization process is a highly generic and inexpensive way to devise functional nanostructured polymer surfaces for selective biomolecule interactions.[21,22] Valsesia et al. successfully implemented this integrated system to fabricate nanocraters of poly(acrylic acid) (carboxyl moieties) surrounded by a matrix of poly(ethylene glycol) (PEG).[23] The surface chemistry of the polymer nanopatterns can be tuned either by the choice of the process vapor employed for plasma polymerization or by post-treatment of functional groups present on the plasma-polymer surface for specific applications.

While self-assembled monolayers of monocomponent spherical particles thus provide useful masks for plasma patterning of substrates, they impose some restrictions on dimensions and spatial patterns that can be produced.[24] Moreover, such crystal masks are produced with several defects, and colloidal assembly below 100 nm particles leads to either irregular arrangement of nanoparticles or few μm^2 ordered domain sizes, thus severely affects the uniformity of the resultant plasma patterns produced from such masks. These problems can be overcome if self-assembled binary colloidal crystals (BCCs) are used as masks. BCCs comprising a mixture of two kinds of particles of different sizes enable the design and fabrication of substantially more flexible masks, particularly when large particles can assist the self-assembly and colloidal stability of very small particles in-between the large ones. Such a binary approach may yield patterns with tunable geometries on the substrate surface of a size amenable to single-protein immobilization onto such islands of modified surface areas via masking. Here, we report, for the first time, the use of plasma polymerization through BCC masks as a versatile, simple, and rapid approach for the generation of functional polymer patterns on various hydrophilic substrates, with a size scale from several micrometers to sub-100 nanometers. In the past decade, several methods have been introduced for the controlled growth of BCCs.[25–28] We have used an area-confinement evaporation-induced assembly method to produce BCCs from very low volume fractions of employed colloidal particles. The plasma polymerization process then enables generation of chemically functional surfaces of tunable properties from a wide range of volatile organic vapors (as a plasma process gas) and by controlling the operating parameters. In this study, we have used *n*-heptylamine (HA) as a "monomer" for plasma polymerization, with the intention of creating patterned amine functionalized regions on substrates. To proof the validity of these surfaces for biomolecular patterning, these amine regions have been used as platforms for further additional chemical functionalization, such as grafting of *m*-poly(ethylene glycol) propionaldehyde (m-PEG-PALD) by reductive animation to create PEGylated surface areas resistant to nonspecific protein adsorption.[29] This integrated plasma-based approach is applicable to most solid substrates.

2. Results and Discussion

The principle is shown schematically in **Figure 1**. The first step involves drop-casting of the colloidal suspension onto a clean hydrophilic substrate area enclosed by a rubber ring (Figure 1a). The colloidal suspension is prepared from particles of different sizes and chemical functionality in pure MilliQ water. The mechanism of their formation is a multistep process and is based on the interplay of various interactions such as electrostatic, capillary, convective flow, and entropic forces. The electrostatic forces acting between the particles prevent their aggregation during the assembly formation on the substrate. As evaporation processes proceed, the immersion capillary forces arise when a concave liquid layer is formed at the center of the ring and deforms around the large particles, i.e., the thickness of the liquid layer at center is less than the particle diameter (Figure 1b).[30] The magnitude of capillary force is significantly higher than electrostatic forces, thus bringing the large particles close to each other.[31] Once loosely packed regions are nucleated, a concave meniscus forms between the large particles. Evaporation from these meniscuses results in increases in local radius of curvature, and thus induces a local build-up of capillary pressure. This directs a liquid flux containing electrostatically stabilized particles from the thicker portion of the liquid, where the pressure is very high, towards the low-pressure region. Both particles move towards nucleated regions due to convective or hydrodynamic forces.[30] When the local colloidal concentration exceeds a critical concentration at the center of the ring, entropic forces dominate and lead to ordered crystal growth after complete evaporation (Figure 1c).

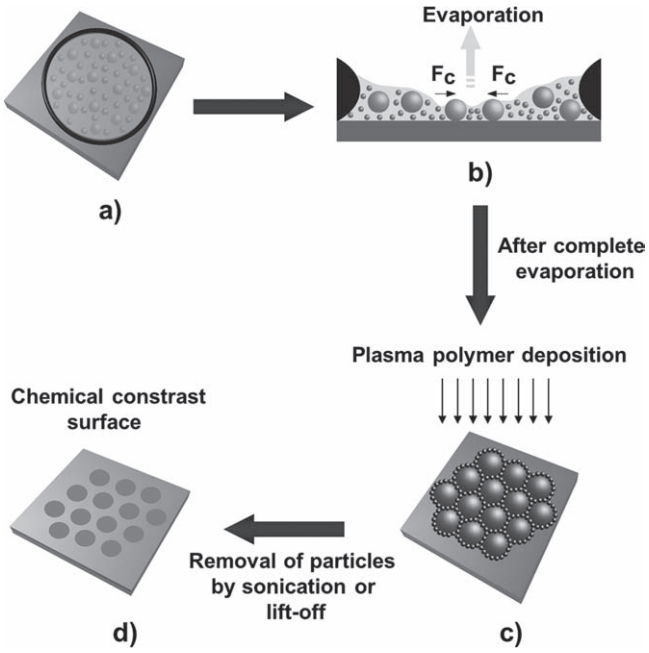

Figure 1. Schematic illustration of BCC fabrication and plasma-polymer patterning. a) A suspension of colloidal nanoparticles is spread inside a rubber ring. b) Nucleation of the order region due to attractive lateral capillary forces (F_c, shown by arrows) when the height of the liquid layer at the is less than the large particle diameter. c) Binary colloidal crystal formation upon complete evaporation and plasma polymerization over binary colloidal crystal mask. d) Chemical contrast patterned surface (plasma polymer against silicon/glass) after particle removal by either sonication or lift-off.

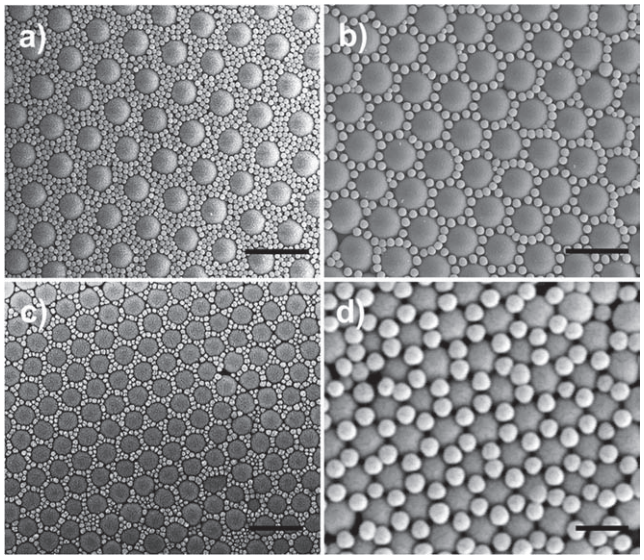

Figure 2. SEM images of BCCs at different γ: a) 2 μm COOH-PS and 200 nm NH_2-PS, $\gamma = 0.10$, scale bar = 3 μm; b) 2 μm COOH-PS and 400 nm NH_2-PS, $\gamma = 0.20$, scale bar = 3 μm; c) 200 nm NH_2-PS and 50 nm COOH-Silica, $\gamma = 0.25$, scale bar = 500 nm; d) 200 nm NH_2-PS and 110 nm NH_2-PS, $\gamma = 0.55$, scale bar = 300 nm.

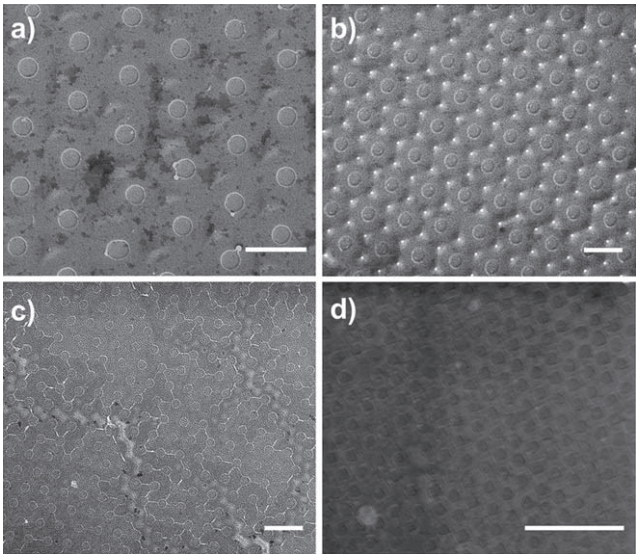

Figure 3. SEM images of HA plasma-polymer patterning using BCCs mask: a) 2 μm plain-silica and 200 nm NH_2-PS, $t = 8$ min, scale bar = 2 μm; b) 1 μm SO_4-PS and 110 nm NH_2-PS, $t = 12$ min, scale bar = 1 μm; c) 500 nm SO_4-PS and 50 nm COOH-Silica, $t = 6$ min, scale bar = 1 μm; d) 200 nm NH_2-PS and 50 nm COOH-Silica, $t = 4$ min, scale bar = 1 μm.

The crystallization proceeds from the center to the edge of the ring and continues until complete evaporation of liquid has occurred.

Notably, binary colloidal assemblies of different crystal structure types were observed, depending on the size ratios (γ = small/large) of the particles utilized; an example is shown in **Figure 2**. At very low γ (0.10), for example an assembly generated from 2 μm, in diameter, carboxyl-polystyrene (COOH-PS) and 200 nm amine-polystyrene (NH_2-PS) showed uniform distribution of small particles around the large particles arranged locally in hexagonal arrays (Figure 2a). As γ increases from 0.20 to 0.25, the number of small particles in between the large particles decreased (Figure 2b,c). A different crystal structure was observed as γ reached 0.50, with small particles (100 nm NH_2-PS) settling over voids within the large-particle (200 nm NH_2-PS) monolayer (Figure 2d). Therefore, this method efficiently generates a wide range of binary nanocolloidal crystals over several cm^2 regions on a substrate. Here, we only focus on BCC assembly obtained at $\gamma = 0.10$ to create plasma-polymer patterned surfaces.

A layer of amine plasma polymer was deposited using different deposition times (t), with a BCC acting as a mask to yield a plasma-polymer pattern on the substrate after removal of the particles by sonication (Figure 1d). Ambipolar diffusion of excited species within the plasma glow above the BCC, through the voids in the BCC, facilitates growth of the plasma-polymer layer underneath the smaller particles. Scanning electron microscopy (SEM) images (**Figure 3**) provide evidence for the plasma-polymerized HA patterns on a silicon substrate using various BCC masks. With longer deposition times there is clearer contrast between the silicon and plasma-polymer regions. The samples had to be coated with a few nm of platinum to combat sample surface charging, and this Pt coating reduces the detectability of very thin plasma-polymer patterns. The plasma-polymerized HA pattern generated using a BCC with 2 μm plain-silica and 200 nm NH_2-PS particles displayed lower height areas of ≈600 nm diameter located in an array corresponding to the original array of the large particles (Figure 3a). These depressions thus result from the shadowing exerted by the large particles, but it is noteworthy that their diameter is less than the diameter of the shadowing particles. This effect is thought to be due to diffusion that enables plasma-gas components to undergo some "sideways" movement and film formation underneath "ledges" created by particles. The plasma deposition process is not a straight line-of-sight process due to significant random diffusion in the moderate pressure vacuum of the plasma polymerization process in addition to the "vertical" diffusion of charged species (electrons, ions) driven by the rf field.

With a BCC comprising 1 μm sulfate-polystyrene (SO_4-PS) and 100 nm NH_2-PS particles, SEM showed the shadowed area to be ≈350 nm in size (Figure 3b). Patterns produced using BCCs consisting of 500 nm SO_4-PS/50 nm COOH-silica and 200 nm NH_2-PS/50 nm COOH-silica were characterized by gap areas of ≈200 and ≈100 nm, respectively (Figure 3c,d). Hence, with this patterning process, well-defined feature sizes down to 100 nm and probably less can be fabricated by using appropriate BCC masks, despite some "sideways" blurring due to random diffusion of film-forming species. Plasma physics suggests that lowering the pressure in the plasma polymerization could reduce such sideways diffusion, if required.[32,33]

It is well known that plasma-polymer deposition depends on various operating conditions during the plasma process, which include parameters such as monomer pressure in the reactor chamber, the discharge glow power, the distance between the electrodes, and the deposition time.[34] In this series of

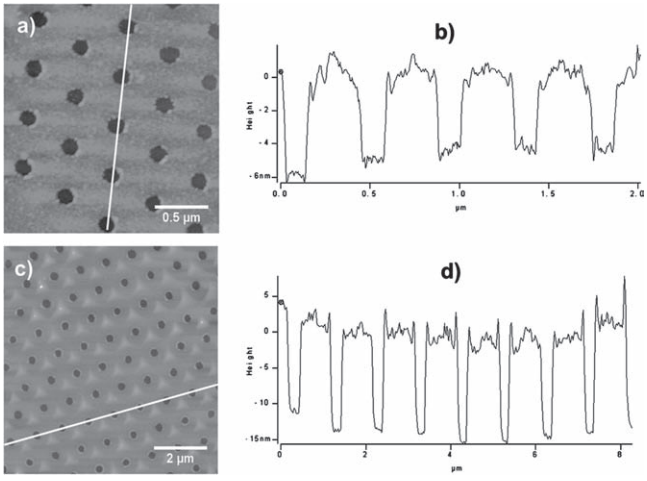

Figure 4. AFM topography images of HA patterned surfaces on silicon substrate. a) Pattern from 500 nm SO_4-PS and 50 nm COOH-Silica (t = 6 min). b) Cross-section analysis of image a; thickness of patterned HApp layer ≈5 nm. c) Pattern from 1 µm SO_4-PS and 110 nm NH_2-PS (t = 8 min). d) Section analysis of image (c); HApp layer thickness ≈13 nm.

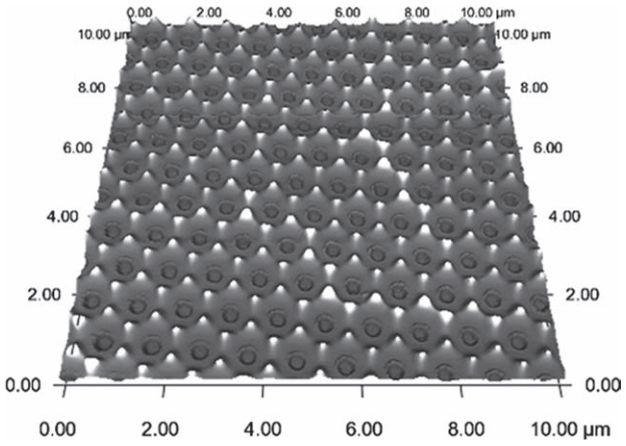

Figure 5. AFM image of egg-carton type HA plasma-polymer pattern at deposition time t = 12 min using a colloidal template comprising 1 µm SO_4-PS and 110 nm NH_2-PS particles.

experiments, all parameters were kept constant and only the deposition time was varied to control the polymer film thickness and study the morphology of the plasma-polymer pattern after removal of the particles. To assess systematically the influence of deposition time on the reduction of the size of the shadowed areas of the polymer pattern, a series of experiments was performed using BCC masks of 2 µm plain-silica/200 nm NH_2-PS, and applying HA polymerization with deposition times for 2 min, 8 min, and 12 min SEM images clearly showed the reduction in pattern size with increasing polymer deposition times from 1.5 µm (t = 2 min) to ~550 nm (t = 12 min) (see the Supporting Information Figure S1). As height information is difficult to extract from such SEM images, the topography of the patterned surfaces was also investigated with atomic force microscopy (AFM) in tapping mode. **Figure 4**a and c shows AFM images of HA nanostructured surfaces obtained with BCC masks of 500 nm SO_4-PS/50 nm COOH-silica, and 1 µm SO_4-PS/100 nm NH_2-PS respectively. Cross-section analysis of the AFM images reveals step heights of 5 nm and 13 nm at these deposition times (Figure 4b and d). Assuming that the (dark) areas directly underneath the large colloid particles are uncoated, the step height represents the coating thickness of the plasma-polymer layer.

Interestingly, we note a change in the pattern formed from a largely 2D pattern to a 3D pattern with the emergence of raised areas centrally between the voids. This becomes more noticeable as the time of plasma deposition, and hence the thickness of the nanopatterned polymer layer increases. It is not surprising that the deposition of polymer is most pronounced in locations furthest from the large colloidal particles. The lighter-coloured dots in Figure 4c correspond to such raised "hilltops" but the effect is seen much more clearly in the AFM image in **Figure 5** with a 12 min plasma deposition, where upon this longer deposition the surface topography has assumed an "egg-carton"-like structure centered on the voids in the coating defined by the large colloid particles. Such periodic "nano-egg-carton" structures can thus be fabricated over areas of several cm^2, potentially providing huge numbers of individual array spots. Therefore, the morphology of nanocolloid plasma-patterned surfaces is highly dependent on deposition time.

We also investigated the influence of different substrates on HA polymer pattern formation and observed similar morphology on hydrophilic glass and polystyrene substrates (see Supporting Information Figure S2). Thus, HA polymer patterning does not depend on substrate chemistry, as is often the case with plasma polymerization.[35] X-ray photoelectron spectroscopy (XPS) was conducted to examine the surface chemistry of HA patterned substrates with 8 min deposition time using a mask of 2 µm plain-silica/200 nm NH_2-PS. The survey spectrum showed the presence of the expected four elements with 80.5% C, 5.5% O, 13.3% N, and 0.54% Si, which arises from the uncoated "holes". The observed chemical composition confirms the deposition of an HA plasma-polymer layer onto the silicon substrate. High-resolution analysis of C 1 s and N 1 s regions were in good agreement with an earlier analysis of HA plasma polymer.[36] The high-resolution C 1 s spectra revealed the presence of three components, which were assigned as aliphatic hydrocarbon (C–C/C–H) at 285.0 eV, amine and ether (C–N/C–O) at 286.3 eV and carbonyl C (C=O) at 287.7 eV (**Figure 6**a). The main component in N 1s indicated the presence of amine (NH_2) functionality at 399.3 eV (Figure 6b). Thus, XPS analysis confirmed a high density of amine groups present on the surface, and these functional surfaces can be employed for specific

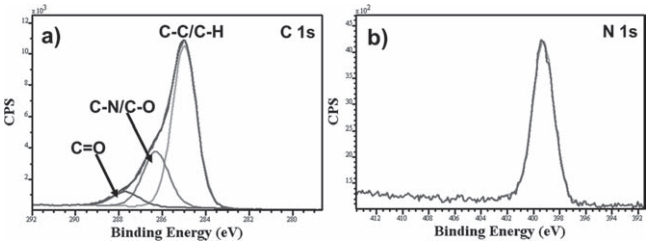

Figure 6. XPS High-resolution spectra of C 1s (a) N 1s (b) regions.

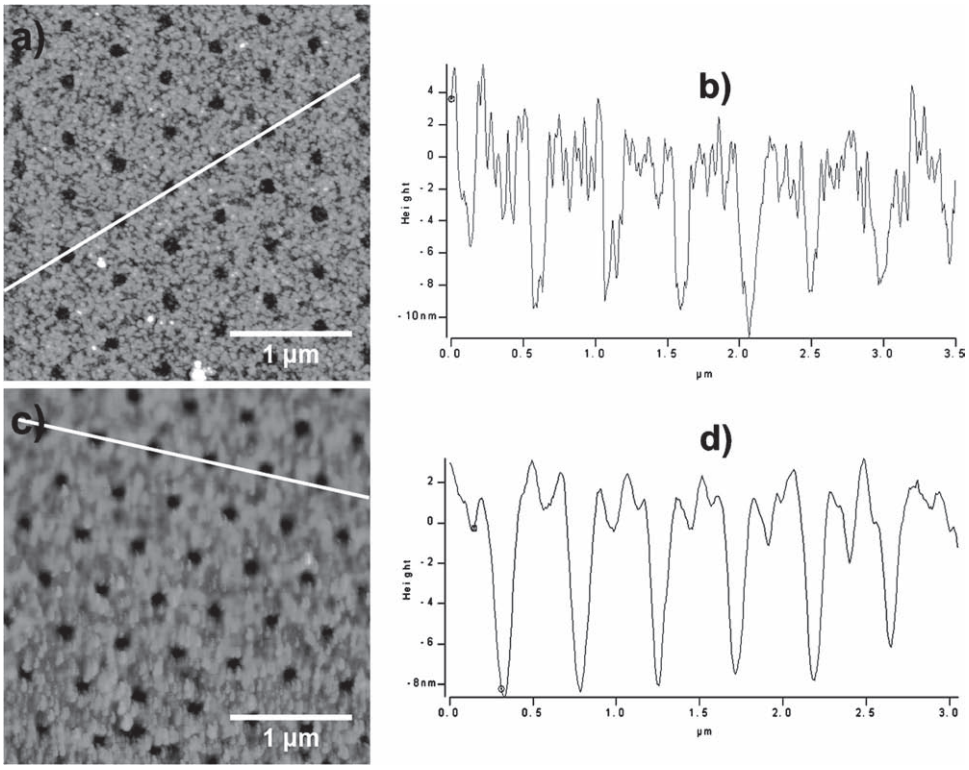

Figure 7. AFM images showing nanometer-scale BSA protein patterning on a HA-patterned surface comprising 500 nm SO_4-PS and 50 nm COOH-ailica after "cloud point" grafting. A) *m*-PEG-PALD grafting; B) section analysis of the image (A) indicating the film thickness ≈9 nm; C) protein nanopatterning; D) section analysis of the image C indicating the reduced film thickness ≈7 nm after protein adsorption.

biomolecule adsorption or covalent coupling for biosensing applications.

The surface chemistry of HA plasma-polymerized patterns can further be modified to graft PEGylated layers, which prevent the nonspecific adsorption of proteins. This was achieved through reductive amination, where *m*-PEG-PALD is covalently linked to amine groups present on the HA surface. A tapping-mode AFM image reveals 2D topography of the *m*-PEG-PALD-grafted plasma-polymerized surface generated from 500 nm SO_4-PS and 50 nm COOH-silica (**Figure 7**a). The grafted surface exhibits the rough morphology rather to without grafted smooth surface, as shown in Figure 4a. Section analysis of the AFM image also confirmed the uniform grafting of the HA plasma-polymerized surface because of the increment in the film thickness from ≈5 nm to ≈9 nm after grafting (compare Figure 4b and Figure 7b). These PEG-grafted surfaces were exposed to a solution of bovine serum albumin (BSA) to evaluate their potential use for the preparation of protein-patterned surfaces. Figure 7c displays the protein-patterned surface, where BSA is expected to selectively adsorb in holes avoiding the protein-resistant PEG-grafted layer. The presence of the proteins inside the holes was again confirmed with section analysis profiles of the AFM image, which revealed the decrease in the depth of a hole from ≈9 nm to ≈7 nm because of the presence of proteins (Figure 7d). The change in thickness of ≈2 nm is less than the dimensions of BSA molecules (14 nm × 4 nm × 4 nm), therefore, it could be possible that some molecules adsorb to the PEG layer. However, previous work shows that this layer is effective at preventing protein adsorption.[29] The minimal changes to surface roughness indicate this is less likely. Also, it is possible that BSA adsorbs at low coverage inside the nanoholes and thus could unfold, giving an average layer thickness less than the molecular dimensions of BSA molecules. Hence, our chemically contrasting surfaces (HA plasma-polymerized against SiO_2) can be used to create bio-nano-patterned surfaces, which may further be scaled down to selective immobilization of single-protein molecules over large areas by use of smaller particles in the initial assembly.

The complementary reverse surface topography patterns can also be created, as shown schematically in **Figure 8**. We observed disclike pattern formation of the HA plasma polymer using a binary colloidal template composed of chemically different materials, e.g., small polystyrene and large silica colloidal particles; the chemical difference is necessary to be able to remove one type of particle selectively. Prior to plasma polymerization, the binary template coated substrate was incubated for 2 to 3 h at 110 °C to melt the small polystyrene particles (Figure 8a). Subsequently, the large silica particles were removed by 1% HF treatment, leaving behind a pattern of melted PS particles, which then served as the template for plasma-polymer deposition (Figure 8b). The disc- or dotlike HA-patterned surface was then imaged after removal of the PS by sonication (Figure 8c). The AFM images in Figure 8d and 8e show the HA disclike pattern formation on silicon substrate. The cross-section analysis

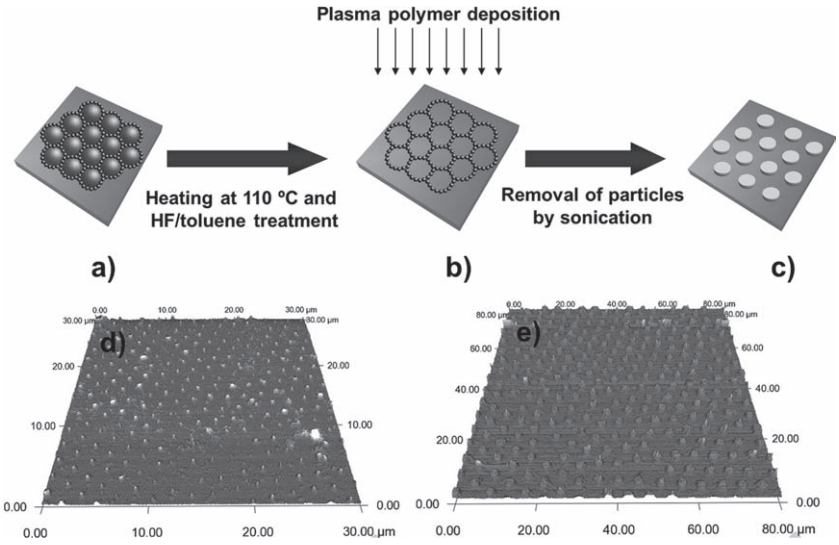

Figure 8. Schematic illustration of disclike polymer pattern formation. a) BCC mask formation. b) Large particle removal after heating and plasma-polymerized-film deposition. c) Plasma-polymer pattern formation after the removal of particles by sonication. AFM images of disclike HA plasma-polymer patterning created after 6 min with masks from 2 μm plain-silica and 200 nm NH_2-PS (d) or 5 μm COOH-PS and 200 nm NH_2-PS (e).

of the AFM images showed ≈80 nm height HA disc pattern of sizes ≈750 nm and ≈2.5 μm, respectively, with masks from 2 μm and 5 μm colloid templates. The method is also able to produce HA patterning over several cm^2 regions on a substrate, and the disc size can be tuned using appropriate BCC masks (see the SEM images in the Supporting Information, Figure S3). This disclike HA-polymer pattern could be employed for cell patterning if their sizes were scaled up to ≈50 μm or more. Our patterning approach also evidence the role of voids in small particles that facilitate plasma deposition underneath them in the before-mentioned plasma-polymer patterns (Figure 3). The heating caused the melting of small particles and consequently suppressed the plasma diffusion in between them, leading to uncoated areas of substantial size. There was no indication of plasma-polymer diffusion through the melted small particle regions.

3. Conclusions

In summary, we have demonstrated the fabrication of various types of binary colloidal crystals depending on the size ratios of the particles. Binary colloidal crystal lithography integrated with a plasma polymerization process has been successfully implemented in order to achieve controlled deposition of a nanopatterned polymer layer onto various substrates. A novel approach has been developed for functional polymer patterning using the lower-size-ratio binary colloidal crystal masks, with features ranging from nanometers to micrometers. The geometry and feature size of the polymer patterns can also be tuned via the deposition time, and a higher deposition time leads to the formation of novel "egg-carton"-type polymer patterning. We also showed the nanometer-scale BSA protein patterning over non-PEGylated regions, which may further be easily expanded to achieve the single-protein patterning. The disclike polymer patterns have also been successfully demonstrated with BCC masks composed of composite materials, where one type of particles is removed before plasma deposition. Other geometries of plasma patterning could be possible if a high-size-ratio BCC was used as a template for polymer deposition. This method offers advantages over previous methods, such as no requirement of complex instrumentation, no use of organic solvents during patterning, no restriction towards particular substrate chemistry, change of geometry with deposition time and composite materials, and inexpensive processes and thus can be further exploited to generate a variety of functional surfaces with a choice of used monomer. Thus, versatile patterning techniques developed in this study might be used for numerous applications including probing cell adhesion, cell patterning, and biological sensing platforms.

4. Experimental Section

Materials: Monodisperse polystyrene particles (sizes from 110 nm to 5 μm), bearing different functional groups (carboxyl, sulfate, and amine) were purchased from Invitrogen (USA). Monodisperse 2 μm plain silica and 50 nm carboxyl silica particles were bought from Polysciences Europe GmbH (Germany), and Kisker GmbH (Germany). These particles were stored at 4 °C. Prior to use the particles were brought to room temperature and sonicated for 30 min. Absolute ethanol (HLPC grade, Sigma–Aldrich), hydrofluoric acid (HF, 40%, Sigma–Aldrich), toluene (≥99.5%, Sigma–Aldrich), *n*-heptylamine (HA, 98%, Fluka), and bovine serum albumin (BSA, lyophilized form, Sigma–Aldrich) were used as received. *m*-Poly(ethylene-glycol) propionaldehyde (*m*-PEG-PALD) with an average molecular weight of 5000 Da was used as received from Laysan Bio, Inc., USA. Sodium cyanoborohydride ($NaCNBH_3$, 90%), potassium sulfate (K_2SO_4, ≥99%), and sodium phosphate dibasic (≥98%) were purchased from Sigma–Aldrich. Boron doped silicon wafers with a diameter of 76.2 mm orientation (100) and a resistivity of 0.0005–0.001 Ω cm were obtained from Virginia Semiconductors (Virginia, USA).

Binary Colloidal Crystals Preparation: Substrates (glass or silicon wafer cut into 1 cm^2 pieces) were cleaned by 15 min sonication, each in solutions of ethanol, toluene, and ethanol, followed by drying with N_2 gas. Polystyrene samples were cut to 1 cm^2 from petri dishes and sonicated in ethanol for 15 min. All substrates were then treated with UV-ozone to achieve a more hydrophilic surface. MilliQ water was used as the solvent during colloidal assembly. The amount of colloidal particles was calculated on the basis of area of substrate encircled by the rubber ring, diameter, and wt% solid content of particles employed. In this method, we used very low amounts of colloidal particles, for instance, to make 200 nm NH_2-PS and 2 μm COOH-PS binary crystals inside a 1 cm diameter rubber ring, 200 nm (0.50 μl) and 2 μm (1.8 μl) particles were mixed in MilliQ water (100 μl, 0.5 μS cm^{-1} conductivity). They were left for 1 h to allow good dispersion. Rubber rings were cleaned thoroughly by sonication in ethanol and MilliQ water for 15 min each. After fixing the rubber ring to the substrate, the colloidal-particle suspension was dropped carefully inside the ring. The substrate was kept in a vacuum desiccator at room temperature until complete evaporation of the solvent, which typically took 2–3 h, depending upon ambient temperature and humidity.

Plasma Reactor: Plasma polymerization was carried out in a custom-built plasma reactor powered by a commercial 13.56 MHz generator (Advanced Energy, USA).[37] HA plasma polymerization was performed under previously optimized conditions of 40 W power and 0.20 Torr pressure in the plasma chamber for various deposition times mentioned in the manuscript.

Grafting and Specific Protein Adsorption: Grafting of *m*-PEG-PALD to HA samples was carried out by reductive amination using $NaCNBH_3$. Grafting was performed under "cloud point" conditions at 60 °C in sodium phosphate buffer (0.1 M) containing K_2SO_4 (11% w/v).[29] The reaction mixture contained $NaCNBH_3$ (3 mg mL^{-1}) and *m*-PEG-PALD (2.5 mg mL^{-1}). The reaction time was 16 h. Samples were then rinsed thoroughly with MilliQ water and finally allowed to equilibrate in MilliQ water for at least 2 h. The freshly grafted samples were exposed to BSA (1 mg mL^{-1}) in phosphate-buffered saline (PBS) for 2 h at room temperature. Samples were rinsed with phosphate buffer and MilliQ water to remove loosely bound proteins.

Characterization Techniques: Field emission scanning electron microscopy (FEI Helios Nanolab Dual Beam) was employed for imaging samples at 5 keV. Prior to imaging, samples were sputtered with Pt for 1 min. An Asylum MFD-3D atomic force microscope (Asylum Research, USA) was used in tapping mode in air with silicon nitrides tips (NT-MDT). XPS analyses were performed using a Kratos Axis Ultra DLD spectrometer (Kratos Analytical, UK), equipped with a monochromatized aluminum X-ray source (Alkα, $h\nu$ = 1486.6 eV) operating at 10 mA and 13 kV (130 W). A hybrid lens (electrostatic and magnetic) mode was employed along with an analysis area of approximately 300 µm × 700 µm. Survey spectra were collected over the range of 0–1100 eV binding energy with an analyser pass energy of 160 eV from nine spots on three samples (three spots per sample). High-resolution spectra of C 1s and N 1s regions were obtained with an analyser pass energy of 20 eV. XPS data were processed with CasaXPS software (Casa Software Ltd., UK).

Supporting Information

Supporting Information is available from the Wiley Online Library or from the author.

Acknowledgements

We thank Marek Jasieniak and Chris Bassell for their scientific discussion and help in experiments. This work was funded through a Danish Research Council Internationalization PhD Stipend and the Ian Wark Research Institute, South University, Adelaide, South Australia, Australia.

Received: July 2, 2010
Published online: December 9, 2010

[1] L. Xiu, S. C. Vemula, M. Jain, S. K. Nam, V. M. Donnelly, D. J. Economou, P. Ruchhoeft, *Nano Lett.* **2005**, *5*, 2563.
[2] Z. Pan, N. Alem, T. Sun, V. P. Dravid, *Nano Lett.* **2006**, *6*, 2344.
[3] A. Kumar, H. A. Biebuyck, G. M. Whitesides, *Langmuir*, **1994**, *10*, 1498.
[4] A. Valsesia, P. Colpo, M. M. Silvan, T. Meziani, G. Ceccone, F. Rossi, *Nano Lett.* **2004**, *6*, 1047.
[5] M. Arnold, E. A. Cavalacanti-Adam, R. Glass, J. Blummel, W. Eck, M. Kantlehner, H. Kessler, J. P. Spatz, *ChemPhysChem* **2004**, *5*, 383.
[6] A. Curtis, M. Riehle, *Phys. Med. Biol.* **2001**, *46*, R47.
[7] L. Kam, W. Shain, J. N. Turner, R. Bizios, *Biomat.* **1999**, *20*, 2343.
[8] D. R. Walt, *Science* **2005**, *308*, 217.
[9] A. S. Blawas, W. M. Reichert, *Biomat.* **1998**, *19*, 595.
[10] S. Sun, G. J. Leggett, *Nano Lett.* **2004**, *4*, 1381.
[11] Y. Xia, G. M. Whitesides, *Annu. Rev. Mater. Sci.* **1998**, *28*, 153.
[12] C. S. Chen, M. Mrksich, S. Huang, G. M. Whitesides, D. E. Ingber, *Science* **1997**, *276*, 5317.
[13] F. Bretagnol, A. Valsesia, t. Sasaki, G. Ceccone, P. Colpo, F. Rossi, *Adv. Mater.* **2007**, *19*, 1947.
[14] H. Gao, N. N. Gosvami, J. Deng, L. T. Tan, M. S. Sander, *Langmuir* **2006**, *22*, 8078.
[15] P. M. Tessier, O. D. Velev, A. T. Kalambur, A. M. Lenhoff, J. F. Rabolt, E. W. Kaler, *Adv. Mater.* **2001**, *13*, 396.
[16] M. Gustavsson, H. Fredriksson, B. Kasemo, Z. Jusys, J. Kaiser, C. Jun, R. J. Bhem, *J. Electroanal. Chem.* **2004**, *568*, 371.
[17] P. Jiang, K. S. Hwang, D. M. Mittlerman, J. F. Bertone, V. L. Colvin, *J. Am. Chem. Soc.* **1999**, *121*, 11630.
[18] P. Jiang, J. F. Bertone, V. L. Colvin, *Science* **2001**, *291*, 453.
[19] H. Agheli, J. Malmstrom, E. M. Arsson, M. Textor, D. S. Sutherland, *Nano Lett.* **2006**, *6*, 1165.
[20] Z. R. Taylor, K. Patel, T. G. Spain, J. C. Keay, J. D. Jernigen, E. S. Sanchez, B. P. Grady, M. B. Johnson, D. W. Schmidtke, *Langmuir* **2009**, *25*, 10932.
[21] S. Mornet, F. Bretagnol, I. Mannelli, A. Valsesia, L. Sirghi, P. Colpo, F. Rossi, *Small* **2008**, *11*, 1919.
[22] L. Ploux, K. Anselme, A. Dirani, A. Ponche, O. Soppera, V. Roucoules, *Langmuir* **2009**, *25*, 8161.
[23] A. Valsesia, P. Colpo, T. Meziani, F. Bretagnol, M. Lejeune, F. Rossi, A. Bouma, M. Garcia-Parajo, *Adv. Funct. Mater.* **2006**, *16*, 1242.
[24] N. J. Trujillo, S. H. Baxamusa, K. K. Gleason, *Chem. Mater.* **2009**, *21*, 742.
[25] K. P. Velikov, C. G. Christova, R. P. A. Dullens, A. van Blaaderen, *Science* **2002**, *296*, 106.
[26] V. Kitaev, G. A. Ozin, *Adv. Mater.* **2003**, *15*, 75.
[27] E. V. Shevchenko, D. V. Talapin, N. A. Kotov, S. O'Brien, C. B. Murray, *Nature* **2006**, *439*, 55.
[28] R. Mukhopadhyay, O. Al-Hanbali, S. Pillai, A. G. Hemmersam, R. L. Meyer, A. C. Hunter, K. J. Rutt, F. Besenbacher, S. M. Moghimi, P. Kingshott, *J. Am. Chem. Soc.* **2007**, *129*, 13390.
[29] P. Kingshott, S. McArthur, H. Thissen, D. G. Castner, H. J. Griesser, *Biomaterials.* **2002**, *23*, 4775.
[30] N. D. Denkov, O. D. Velev, P. A. Kralchevsky, I. B. Ivanov, H. Yoshimura, K. Nagayama, *Nature* **1993**, *26*, 361.
[31] P. A. Kralchevsky, K. Nagayama, *Langmuir* **1994**, *10*, 23.
[32] H. K. Yasuda, *Plasma Process. Polym.* **2005**, *2*, 293.
[33] D. C. Schram, Th. H. J. Bisschops, G. M. W. Kroesen, F. J. de Hoog, *Plasma Phys. Control. Fusion* **1987**, *29*, 1353.
[34] Y. Martin, D. Boutin, P. Vermette, *Thin Solids Films* **2007**, *515*, 6844.
[35] K. S. Siow, L. Britcher, S. Kumar, H. J. Griesser, *Plasma. Process. Polym.* **2006**, *3*, 392.
[36] T. R. Gengenbach, R. C. Chatelier, H. J. Griesser, *Surf. Interface Anal.* **1996**, *24*, 271.
[37] H. J. Griesser, *Vacuum* **1989**, *39*, 485.